

Characterizing and tracking single colloidal particles with video holographic microscopy

Sang-Hyuk Lee,¹ Yohai Roichman,¹ Gi-Ra Yi,² Shin-Hyun Kim,³ Seung-Man Yang,³ Alfons van Blaaderen,⁴ Peter van Oostrum,⁴ and David G. Grier¹

¹*Department of Physics and Center for Soft Matter Research, New York University, New York, NY 10003*

²*Korea Basic Research Institute, Seoul 136-713, Korea*

³*National Creative Research Initiative Center for Integrated Optofluidic Systems and Department of Chemical and Biomolecular Engineering,*

Korea Advanced Institute of Science and Technology, Daejeon, 307-701 Korea

⁴*Soft Condensed Matter, Debye Institute, Utrecht University, 3508 TA Utrecht, The Netherlands*

(Dated: October 27, 2018)

We use digital holographic microscopy and Mie scattering theory to simultaneously characterize and track individual colloidal particles. Each holographic snapshot provides enough information to measure a colloidal sphere's radius and refractive index to within 1%, and simultaneously to measure its three-dimensional position with nanometer in-plane precision and 10 nanometer axial resolution.

In addition to their ubiquity in natural and industrial processes, colloidal particles have come to be prized as building blocks for photonic and optoelectronic devices, as probes for biological and macromolecular processes, and as model systems for fundamental studies of many-body physics. Many of these existing and emerging applications would benefit from more effective methods for tracking colloidal particles' motions in three dimensions. Others require better ways to measure particles' sizes and to characterize their optical properties, particularly if these measurements can be performed on individual particles *in situ*.

This Article demonstrates that images obtained with in-line holographic microscopy^{1,2} can be interpreted with Lorenz-Mie theory^{3,4} to obtain exceptionally precise measurements of individual colloidal spheres' dimensions and optical properties^{5,6} while simultaneously tracking their three dimensional motions with nanometer-scale spatial resolution at video rates⁷. This method works over the entire range of particle sizes and compositions for which Mie scattering theory applies, and requires only a single calibration of the optical train's magnification. Unlike other light scattering techniques for measuring particle size⁸ or refractive index, holographic particle analysis can be applied directly to individual particles in heterogeneous samples and also is compatible with scanned⁹ and holographic¹⁰ optical trapping.

Our holographic analysis instrument is based on a standard inverted optical microscope (Nikon TE-2000U), with a collimated and attenuated HeNe laser (Uniphase 5 mW, $\lambda = 0.632 \mu\text{m}$) replacing the conventional incandescent illuminator and condenser. As indicated schematically in Fig. 1, light scattered by a particle propagates to the microscope's focal plane, where it interferes with the undiffracted portion of the beam. The resulting interference pattern is magnified¹ by the microscope's objective lens (Nikon 100 \times NA 1.4 oil immersion Plan-Apo) and video eyepiece (1.5 \times) onto the sensor of a grey-scale video camera (NEC TI-324AII). This system provides a total magnification of $135 \pm 1 \text{ nm/pixel}$ over a $86 \times 65 \mu\text{m}^2$

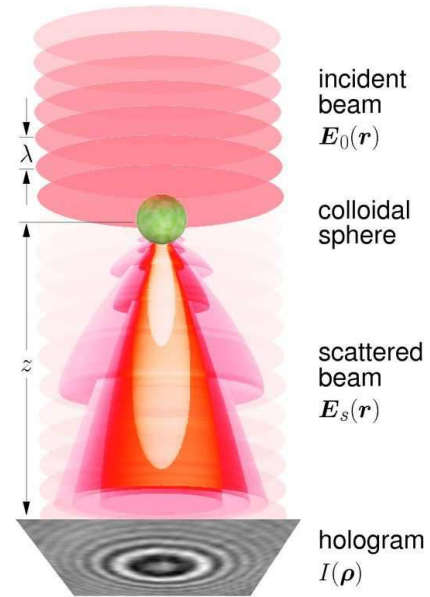


FIG. 1: **Principle of video holographic microscopy.** A colloidal particle scatters a portion $\mathbf{E}_s(\mathbf{r})$ of an initially collimated laser beam $\mathbf{E}_0(\mathbf{r})$. The scattered beam, here represented by 5 calculated iso-amplitude surfaces, interferes with the unscattered portion of the incident beam in the focal plane of a microscope objective, thereby forming an in-line hologram, $I(\boldsymbol{\rho})$.

field of view. Images are recorded as uncompressed digital video at 30 frames/s using a commercial digital video recorder (Pioneer 520HS).

Analyzing these digitized holograms yields the particle's three-dimensional position, \mathbf{r}_p , its radius, a , and its index of refraction, n_p . We assume that the incident field, $\mathbf{E}_0(\mathbf{r}) = u_0(\boldsymbol{\rho}) \exp(ikz) \hat{\mathbf{e}}$, is uniformly polarized in the $\hat{\mathbf{e}}$ direction and varies slowly enough over the size of the particle to be treated as a plane wave propagating along the $\hat{\mathbf{z}}$ direction. Its amplitude $u_0(\boldsymbol{\rho})$ at position $\boldsymbol{\rho} = (x, y)$ in the plane $z = z_p$ of the particle is thus the

same as its amplitude in the focal plane, $z = 0$. The wave propagates along the \hat{z} direction with wave number $k = 2\pi n_m/\lambda$, where λ is the light's wavelength in vacuum and n_m is the refractive index of the medium. For pure water at 25°C, $n_m = 1.3326$ at $\lambda = 0.632 \mu\text{m}$.

The particle at \mathbf{r}_p scatters a portion of the incident field into a highly structured outgoing wave, $\mathbf{E}_s(\mathbf{r}) = \alpha \exp(-ikz_p) u_o(\mathbf{r}_p) \mathbf{f}_s(\mathbf{r} - \mathbf{r}_p)$, where $\alpha \approx 1$ accounts for variations in the illumination, and where $\mathbf{f}_s(\mathbf{r})$ is the Lorenz-Mie scattering function^{3,4,11}, which depends on a , n_p , n_m and λ . The scattered field generally covers a large enough area at the focal plane that the interference pattern,

$$I(\boldsymbol{\rho}) = |\mathbf{E}_s(\mathbf{r}) + \mathbf{E}_0(\mathbf{r})|^2 \Big|_{z=0}, \quad (1)$$

is dominated by long-wavelength variations in $|u_o(\boldsymbol{\rho})|^2$. The resulting distortions have been characterized¹², but were not corrected in previous analyses of $I(\boldsymbol{\rho})$ ^{5,6,7,12,13}. Fortunately, $|u_o(\boldsymbol{\rho})|^2$ can be measured in an empty field of view, and the in-line hologram can be normalized to obtain the undistorted image

$$B(\boldsymbol{\rho}) \equiv \frac{I(\boldsymbol{\rho})}{|u_o(\boldsymbol{\rho})|^2} \quad (2)$$

$$= 1 + \frac{2 \Re\{\mathbf{E}_s(\mathbf{r}) \cdot \mathbf{E}_0^*(\mathbf{r})\}}{|u_o(\boldsymbol{\rho})|^2} + \frac{|\mathbf{E}_s(\mathbf{r})|^2}{|u_o(\boldsymbol{\rho})|^2}, \quad (3)$$

on the plane $z = 0$. If we further assume that the phase of the collimated incident beam varies slowly over the field of view, the normalized image is related to the calculated Mie scattering pattern, $\mathbf{f}_s(\mathbf{r})$, in the plane $z = 0$ by

$$B(\boldsymbol{\rho}) \approx 1 + 2\alpha \Re\{\mathbf{f}_s(\mathbf{r} - \mathbf{r}_p) \cdot \hat{\mathbf{e}} e^{-ikz_p}\} + \alpha^2 |\mathbf{f}_s(\mathbf{r} - \mathbf{r}_p)|^2. \quad (4)$$

Equation (4) can be fit to measured holograms by treating the particle's three-dimensional position, its radius and its refractive index as free parameters. Previous studies fit non-normalized holograms to phenomenological models^{6,13,14,15,16,17} or Mie scattering theory¹⁸ for some of these quantities, but never all five. Because errors in the adjustable parameters are strongly correlated, failing to optimize them all simultaneously yields inaccurate results. Fitting instead to the full Lorenz-Mie theory^{3,4,11,12,19,20} provides more information with greater precision.

Numerical fits to digitized and normalized holographic images were performed with the Levenberg-Marquardt nonlinear least-squares minimization algorithm^{21,22,23} using the camera's measured signal-to-noise ratio to estimate single-pixel errors. The χ^2 deviates for all of the fits we report are of order unity, so that the calculated uncertainties in the fit parameters accurately reflect their precision^{21,23,24}. These estimates incorporate the estimated covariance of the adjustable parameters, so that they also may be interpreted as the resolution of each parameter²⁴.

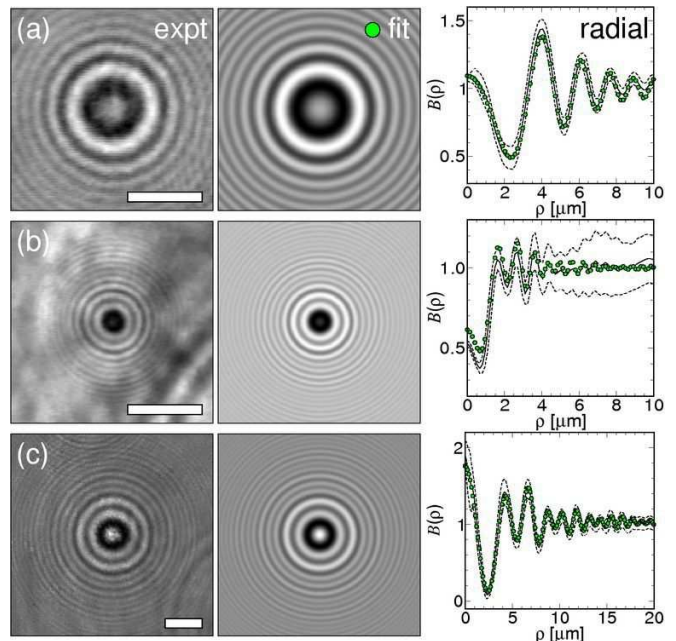


FIG. 2: **Fitting to normalized holograms.** (a) Normalized hologram $B(\boldsymbol{\rho})$, numerical fit to Eq. (4), and azimuthally averaged radial profile $B(\rho)$ for a $1.43 \mu\text{m}$ diameter polystyrene sphere in water at $z_p = 22.7 \mu\text{m}$. All scale bars indicate $10 \mu\text{m}$. Curves in the radial profile are obtained from experimental data, discrete points were obtained from the fit. (b) Data for a $1.45 \mu\text{m}$ diameter TiO_2 sphere dispersed in immersion oil ($n_m = 1.515$) at $z_p = 7.0 \mu\text{m}$ (c) Data for a $4.5 \mu\text{m}$ diameter SiO_2 sphere in water at $z_p = 38.8 \mu\text{m}$.

Because the laser's wavelength and the medium's refractive index are both known, the only instrumental calibration is the overall magnification. This contrasts with other three-dimensional particle tracking techniques^{1,2,13,25,26,27}, which require independent calibrations for each type of particle, particularly to track particles in depth.

The image in Fig. 2(a) shows the normalized hologram, $B(\boldsymbol{\rho})$, for a polystyrene sulfate sphere dispersed in water at height $z_p = 22.7 \mu\text{m}$ above the focal plane. This sphere was obtained from a commercial sample with a nominal diameter of $2a = 1.48 \pm 0.03 \mu\text{m}$ (Bangs Labs, Lot PS04N/6064). The camera's electronic shutter was set for an exposure time of 0.25 msec to minimize blurring due to Brownian motion²⁸. After normalizing the raw 8-bit digitized images, each pixel contains roughly 5 significant bits of information. The numerical fit to $B(\boldsymbol{\rho})$ faithfully reproduces not just the position of the interference fringes, but also their magnitudes. The quality of the fit may be judged from the azimuthal average; the solid curve is an angular average about the center of $B(\boldsymbol{\rho})$, the dashed curves indicate the standard deviations of the average, and the discrete points are obtained from the fit.

The fit value for the radius, $a = 0.73 \pm 0.01 \mu\text{m}$, falls in the sample's specified range, which reflected a lower

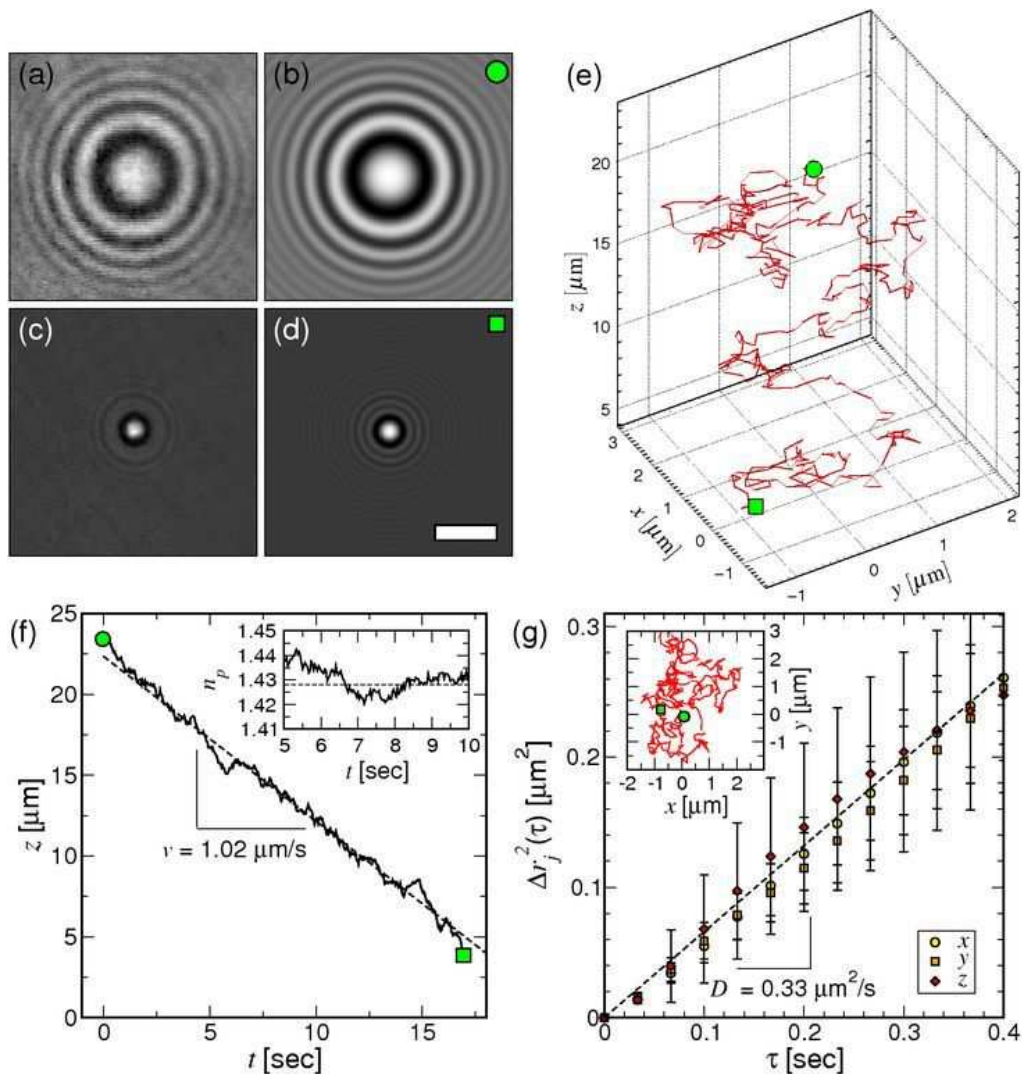


FIG. 3: **Holographic tracking of a sedimenting colloidal silica sphere.** (a) and (c) DHM images of the sphere at the beginning and end of its trajectory, respectively. The scale bar indicates $5 \mu\text{m}$. (b) and (d) Fits to Eq. (4). (e) Three-dimensional trajectory with starting point (circle) and end point (square) labeled. (f) $z(t)$, showing thermal fluctuations about uniform sedimentation. Inset: The fit refractive index is independent of position. (g) Mean-square positional fluctuations display Einstein-Smoluchowsky scaling in x , y and z .

bound of $0.69 \pm 0.07 \mu\text{m}$ obtained with a Beckman Z2 Coulter Counter and an upper bound of $0.76 \pm 0.08 \mu\text{m}$ obtained by analytical centrifugation. Agreement between the quoted and measured particle size suggests that the present measurement's accuracy is comparable to its precision. In that case, both precision and accuracy surpass results previously obtained⁶ through analysis of $I(\rho)$. The trajectory-averaged value for the refractive index, $n_p = 1.55 \pm 0.03$, also is consistent with the properties of polystyrene colloid inferred from light scattering measurements on bulk dispersions²⁹.

Comparable precision in measuring a single particle's refractive index has been achieved by analyzing a colloidal particle's dynamics in an optical trap³⁰. This method only can be applied to particles with comparatively small refractive indexes, however, because particles

with relative refractive indexes greater than $n_p \approx 1.3 n_m$ are difficult to trap. Holographic characterization, by contrast, requires only a single holographic snapshot rather than an extensive time series, does not require optical trapping, and so does not require separate calibration of the trap, and is effective over a wider range of particle sizes and refractive indexes.

The corresponding data in Fig. 2(b) were obtained for a $1.45 \mu\text{m}$ diameter TiO_2 sphere at $z_p = 7 \mu\text{m}$ above the focal plane. This sample was synthesized from titanium tetraethoxide and was heat-treated to increase its density³¹. Strong forward scattering by such high-index particles gives rise to imaging artifacts unless the medium is index matched to the cover slip. Dispersing the particle in immersion oil ($n_m = 1.515$) eliminates these artifacts, but introduces spherical aberration for

the lens we used, which must be corrected³² to obtain reliable results. The fit diameter of $1.45 \pm 0.03 \mu\text{m}$ and refractive index of 2.01 ± 0.05 are consistent with results obtained by electron microscopy and bulk light scattering, respectively. This result is noteworthy because no other single-particle characterization method works for such high refractive indexes.

The data in Fig. 2(c) show results for a nominally $5 \mu\text{m}$ silica sphere (Bangs Labs, Lot SS05N/4364) dispersed in water at $z_p = 38.8 \mu\text{m}$ above the focal plane. The fit refractive index, $n_p = 1.434 \pm 0.001$, is appropriate for porous silica and the diameter, $a = 4.51 \pm 0.01 \mu\text{m}$ agrees with the $4.82 \pm 0.59 \mu\text{m}$ value obtained for this sample with a Beckman Z2 Coulter Counter.

The same fits resolve the particle's position with a precision of 1 nm in-plane and 10 nm along the optical axis. This substantially improves upon the typical 10 nm in-plane accuracy obtained with standard particle tracking techniques with the same microscope and camera²⁵. The difference can be ascribed to the larger number of pixels subtended by a holographic image, and to the images' strong intensity gradients, which constrain the fits. The estimated 10 nm axial resolution surpasses results obtained with morphometric axial particle tracking^{1,2,25} by a factor of ten.

Nanometer-scale tracking resolution can be obtained under conventional illumination, but requires detailed calibrations for each particle³³. Still better in-plane spatial resolution can be obtained at much higher bandwidths through back-focal-plane interferometric methods³⁴, but also require accurate calibrations with piezo translators. Total internal reflection microscopy (TIRM) similarly offers sub-nanometer axial resolution^{35,36}, but performs no better than conventional imaging methods for in-plane tracking.

An additional benefit of holographic imaging over other particle-tracking techniques is its very large depth of focus. Our system provides useful data over a range of more than $100 \mu\text{m}$, which contrasts with the $\pm 3 \mu\text{m}$ useful depth of focus using conventional illumination³³ and the 100 nm range of TIRM^{35,36}.

Holographic video microscopy lends itself to three-dimensional particle tracking, as the data in Fig. 3 demonstrate for a colloidal silica sphere (Bangs Labs, Lot SS04N/5252) dispersed in water. This particle was lifted $30 \mu\text{m}$ above the focal plane with an optical tweezer, and then released and allowed to sediment. The images in Fig. 3(a) and (c) show the particle near the beginning of its trajectory and near the end. Fits to Eq. (4) are shown in Figs. 3(b) and (d).

The particle's measured trajectory in 1/30 s intervals during 15 s of its descent is plotted in Fig. 3(e). Its vertical position $z(t)$, Fig. 3(f), displays fluctuations about a uniform sedimentation speed, $v = 1.021 \pm 0.005 \mu\text{m/s}$. This provides an estimate for the particle's density through $\rho_p = \rho_m + 9\eta v / (2a^2 g)$, where $\rho_m = 0.997 \text{ g/cm}^3$ is the density of water and $\eta = 0.0105 \text{ P}$ is its viscosity at $T = 21^\circ\text{C}$, and where $g = 9.8 \text{ m/s}^2$ is the acceleration

due to gravity. The fit value for the particle's radius, at $a = 0.729 \pm 0.012 \mu\text{m}$, remained constant as the particle settled. This value is consistent with the manufacturer's specified radius of $0.76 \pm 0.04 \mu\text{m}$, measured with a Beckman Z2 Coulter Counter. Accordingly, we obtain $\rho_p = 1.92 \pm 0.02 \text{ g/cm}^3$, which is a few percent smaller than the manufacturer's rating for the sample. However, the fit value for the refractive index, $n_p = 1.430 \pm 0.007$, also is 1.5% below the rated value, suggesting that the particle is indeed less dense than specified.

The mean-square displacements, $\Delta r_j^2(\tau) = \langle (r_j(t+\tau) - r_j(t))^2 \rangle$, of the components of the particle's position provide additional consistency checks. As the data in Fig. 3(g) show, fluctuations in the trajectory's individual Cartesian components agree with each other, and all three display linear Einstein-Smoluchowsky scaling, $\Delta r_j^2(\tau) = 2D\tau$, with a diffusion coefficient $D = 0.33 \pm 0.03 \mu\text{m}^2/\text{s}$. This is consistent with the anticipated Stokes-Einstein value, $D_0 = k_B T / (6\pi\eta a) = 0.30 \pm 0.02 \mu\text{m}^2/\text{s}$, where k_B is Boltzmann's constant. Using the methods of Ref.²⁸, we then interpret the offsets obtained from linear fits to $\Delta r_j^2(t)$ to be consistent with no worse than 1 nm accuracy for in-plane positions and 10 nm for axial positions throughout the trajectory. The optical characterization of the particle's properties thus is consistent with the particle's measured dynamics.

We have successfully applied holographic characterization to colloidal spheres as small as 100 nm in diameter and as large as $10 \mu\text{m}$. Unlike model-based analytical methods, fitting to the exact Lorenz-Mie scattering theory is robust and reliable over a far wider range of particle sizes, provided that care is taken to maintain numerical stability in calculating $\mathbf{f}_s(\mathbf{r})$ ^{3,19,20}. Such numerical implementations have been reported for particles as small as a few nanometers and as large as a few millimeters, with relative refractive index ratios from less than $m = 0.1$ to over 10, and with large imaginary refractive indexes. In all cases, the instrumental magnification and field of view must be selected to fit the sample.

The principal limitations of the six-parameter model in Eq. (4) are the assumptions that the scatterer is homogeneous and isotropic, and that its interface is sharp. These assumptions can be relaxed at the cost of increased complexity and reduced numerical robustness. For example, analytical results are available for core-shell particles³, and for particles with more complex shapes^{3,11}, such as ellipsoids, spherical clusters and cylindrical nanowires. All such elaborations involve additional adjustable parameters and thus are likely to pose computational challenges.

We have demonstrated that a single snapshot from an in-line holographic microscope can be used to measure a colloidal sphere's position and size with nanometer-scale resolution, and its refractive index with precision typically surpassing 1 percent.

A video stream of such images therefore constitutes a powerful six-dimensional microscopy for soft-matter and

biological systems. Holographic particle tracking is ideal for three-dimensional microrheology, for measuring colloidal interactions and as force probes for biophysics. The methods we have described can be applied to tracking large numbers of particles in the field of view simultaneously for highly parallel measurements. Real-time single-particle characterization and tracking of large particle ensembles will be invaluable in such applications as holographic assembly of photonic devices^{37,38}. Applied to more highly structured samples such as biological cells and colloidal heterostructures, they could be

used as a basis for cytometric analysis or combinatorial synthesis³⁹.

This work was supported by the National Science Foundation under Grant Number DMR-0606415. SHL acknowledges support of the Kessler Family Foundation. GRY was supported by KBSI grant (N27073). KSH and SMY have been supported by the NCRI Center for Integrated Optofluidic Systems of MOST/KOSEF. We are grateful to Ahmet Demirörs for synthesizing the 1.4 μm diameter TiO_2 particles.

-
- ¹ J. Sheng, E. Malkiel and J. Katz. “Digital holographic microscope for measuring three-dimensional particle distributions and motions.” *Appl. Opt.* **45**, 3893–3901 (2006).
- ² S.-H. Lee and D. G. Grier. “Holographic microscopy of holographically trapped three-dimensional structures.” *Opt. Express* **15**, 1505–1512 (2007).
- ³ C. F. Bohren and D. R. Huffman. *Absorption and Scattering of Light by Small Particles* (Wiley Interscience, New York, 1983).
- ⁴ P. W. Barber and S. C. Hill. *Light Scattering by Particles: Computational Methods*, vol. 2 of *Advanced Series in Applied Physics* (World Scientific, New Jersey, 1990).
- ⁵ A. K. Ray, A. Souyri, E. J. Davis and T. M. Allen. “Precision of light scattering techniques for measuring optical parameters of microspheres.” *Appl. Opt.* **30**, 3974–3983 (1991).
- ⁶ L. Denis, C. Fournier, T. Fournel, C. Ducottet and D. Jeulin. “Direct extraction of the mean particle size from a digital hologram.” *Appl. Opt.* **45**, 944–952 (2006).
- ⁷ D. Moreno, F. M. Santoyo, J. A. Guerrero and M. Funes-Gallanzi. “Particle positioning from charge-coupled device images by the generalized Lorenz-Mie theory and comparison with experiment.” *Appl. Opt.* **39**, 5117–5124 (2000).
- ⁸ R. Xu. *Particle Characterization: Light Scattering Methods* (Springer, New York, 2002).
- ⁹ K. Sasaki, M. Koshio, H. Misawa, N. Kitamura and H. Masuhara. “Pattern formation and flow control of fine particles by laser-scanning micromanipulation.” *Opt. Lett.* **16**, 1463–1465 (1991).
- ¹⁰ D. G. Grier. “A revolution in optical manipulation.” *Nature* **424**, 810–816 (2003).
- ¹¹ M. I. Mishchenko, L. D. Travis and A. A. Lais. *Scattering, Absorption, and Emission of Light by Small Particles* (Cambridge University Press, New York, 2002).
- ¹² Y. Pu and H. Meng. “Intrinsic aberrations due to Mie scattering in particle holography.” *J. Opt. Soc. Am. A* **20**, 1920–1932 (2003).
- ¹³ Y.-K. Park, G. Popescu, K. Badizadegan, R. R. Dasari and M. S. Feld. “Fresnel particle tracing in three dimensions using diffraction phase microscopy.” *Opt. Lett.* **32**, 811–813 (2007).
- ¹⁴ B. J. Thompson. “Holographic particle sizing techniques.” *J. Phys. E: Sci. Instrum.* **7**, 781–788 (1974).
- ¹⁵ S. Soontaranon, J. Widjaja and T. Asakura. “Improved holographic particle sizing by using absolute values of the wavelet transform.” *Opt. Commun.* **240**, 253–260 (2004).
- ¹⁶ S. L. Pu, D. Allano, B. Patte-Rouland, M. Malek, D. Lebrun and K. F. Cen. “Particle field characterization by digital in-line holography: 3D location and sizing.” *Experiments in Fluids* **39**, 1–9 (2005).
- ¹⁷ J. A. Guerrero-Viramontes, D. Moreno-Hernández, F. Mendoza-Santoyo and M. Funes-Gallanzi. “3D particle positioning from CCD images using the generalized Lorenz-Mie and Huygens-Fresnel theories.” *Meas. Sci. Technol.* **17** (2006).
- ¹⁸ S. A. Alexandrov, T. R. Hillman and D. D. Sampson. “Spatially resolved Fourier holographic light scattering angular spectroscopy.” *Opt. Lett.* **30**, 3305–3307 (2005).
- ¹⁹ W. J. Wiscombe. “Improved Mie scattering algorithms.” *Appl. Opt.* **19**, 1505–1509 (1980).
- ²⁰ H. Du. “Mie-scattering calculation.” *Appl. Opt.* **43**, 1951–1956 (2004).
- ²¹ J. J. Moré, B. S. Garbow and K. E. Hillstom. “User Guide for MINPACK-1.” Tech. Rep. ANL-80-74, Argonne National Laboratory, Argonne, IL (1980).
- ²² J. J. Moré. “The Levenberg-Marquardt Algorithm: Implementation and Theory.” In “Numerical Analysis,” edited by G. A. Watson, Lecture Notes in Mathematics 630 (Springer-Verlag, Berlin, 1977).
- ²³ P. E. Gill and W. Muray. “Algorithms for the solution of the nonlinear least-squares problem.” *SIAM J. Numer. Anal.* **15**, 977–992 (1978).
- ²⁴ J. E. Dennis and R. B. Schnabel. *Numerical Methods for Unconstrained Optimization and Nonlinear Equations*. No. 16 in Classics in applied mathematics (SIAM, Philadelphia, 1996).
- ²⁵ J. C. Crocker and D. G. Grier. “Methods of digital video microscopy for colloidal studies.” *J. Colloid Interface Sci.* **179**, 298–310 (1996).
- ²⁶ A. Pralle, M. Prummer, E. L. Florin, E. H. K. Stelzer and J. K. H. Horber. “Three-dimensional high-resolution particle tracking for optical tweezers by forward scattered light.” *Microscopy Research and Technique* **44**, 378–386 (1999).
- ²⁷ M. Speidel, A. Jonáš and E.-L. Florin. “Three-dimensional tracking of fluorescent nanoparticles with subnanometer precision by use of off-focus imaging.” *Opt. Lett.* **28**, 69–71 (2003).
- ²⁸ T. Savin and P. S. Doyle. “Role of finite exposure time on measuring an elastic modulus using microrheology.” *Phys. Rev. E* **71**, 041106 (2005).
- ²⁹ X. Ma, J. Q. Lu, R. S. Brock, K. M. Jacobs, P. Yang and H. Xin-Hua. “Determination of complex refractive index of polystyrene microspheres from 370 to 1610 nm.” *Phys.*

- Med. Biol.* **48**, 4165–4172 (2003).
- ³⁰ G. Knöner, S. Parkin, T. A. Nieminen, N. R. Heckenberg and H. Rubinsztein-Dunlop. “Measurement of the index of refraction of single microparticles.” *Phys. Rev. Lett.* **97** (2006).
- ³¹ S. Eiden-Assmann, J. Widoniak and G. Maret. “Synthesis and characterization of porous and nonporous monodisperse colloidal TiO₂ particles.” *Chem. Mater.* **16** (2004).
- ³² Y. Roichman, A. S. Waldron, E. Gardel and D. G. Grier. “Performance of optical traps with geometric aberrations.” *Appl. Opt.* **45**, 3425–3429 (2005).
- ³³ C. Gosse and V. Croquette. “Magnetic tweezers: Micromanipulation and force measurement at the molecular level.” *Biophys. J.* **82**, 3314–3329 (2002).
- ³⁴ F. Gittes and C. F. Schmidt. “Interference model for back-focal-plane displacement detection in optical tweezers.” *Opt. Lett.* **23**, 7–9 (1998).
- ³⁵ M. A. Brown and E. J. Staples. “Measurement of absolute particle-surface separation using total internal reflection microscopy and radiation pressure forces.” *Langmuir* **6**, 1260–1265 (1990).
- ³⁶ D. C. Prieve and N. A. Frej. “Total internal reflection microscopy: A quantitative tool for the measurement of colloidal forces.” *Langmuir* **6**, 396–403 (1990).
- ³⁷ G. Sinclair, P. Jordan, J. Courtial, M. Padgett, J. Cooper and Z. J. Laczik. “Assembly of 3-dimensional structures using programmable holographic optical tweezers.” *Opt. Express* **12**, 5475–5480 (2004).
- ³⁸ Y. Roichman and D. G. Grier. “Holographic assembly of quasicrystalline photonic heterostructures.” *Opt. Express* **13**, 5434–5439 (2005).
- ³⁹ A. P. R. Johnston, B. J. Battersby, G. A. Lawrie, L. K. Lambert and M. Trau. “A mechanism for forming large fluorescent organo-silica particles: Potential supports for combinatorial synthesis.” *Chem. Mater.* **18**, 6163–6169 (2006).